Eclipta Journals

RESEARCH

Real-Time Kick State Estimation from Sparse Surface Measurements via Thermodynamic Reduced-Order Modeling and Bayesian Data Assimilation

Hammad Raza,[1] Saad Mehmood,[2] and Usman Qureshi[3]

[1]Kohat University of Science and Technology, Bannu Road No. 14, Kohat, Khyber Pakhtunkhwa, Pakistan
[2]University of Turbat, Gwadar Highway No. 7, Turbat, Balochistan, Pakistan
[3]Gulzar-e-Quaid Block 4, Lahore, Punjab, Pakistan

Abstract

Drilling operations routinely encounter uncertain pore-pressure environments in which a narrow margin separates stable overbalanced circulation from an underbalanced influx event. Because downhole instrumentation is often limited, operational decisions are frequently made using sparse surface measurements such as standpipe pressure, choke pressure, flow-out, and pit volume. These signals are informative but non-unique, since multiple downhole states can map to similar surface responses when compressibility, slip, friction, and transient boundary conditions interact. This paper presents a technical framework for real-time kick characterization and control that couples a thermodynamic two-phase annular flow model with a reduced-order discretization and a Bayesian data assimilation layer tailored to surface-only observability. The core contribution is an inference-stable state-space formulation that explicitly represents free-gas migration, dissolution and exsolution in non-aqueous fluids, and pressure-loss evolution under dynamic actuation, while remaining computationally tractable for online use. A sequential ensemble-based estimator reconstructs latent influx parameters such as entry depth, influx rate history, and gas holdup distribution from noisy surface streams, and propagates calibrated uncertainty into a decision module that selects backpressure trajectories consistent with operational constraints. The method is evaluated through numerical experiments spanning circulating and shut-in transients, heterogeneous frictional regimes, and solubility-sensitive mud systems. Results indicate that the proposed approach reduces detection latency while providing physically interpretable posterior distributions for influx size and location, enabling risk-aware well-control actions without requiring dense downhole sensing.

1. Introduction

Gas influx events during drilling remain a central source of non-productive time and safety risk because the annulus is a large, distributed, multiphase system observed through a small number of surface channels [1]. The operational reality is that the most accessible measurements are typically pressures at or near the surface, pump and choke variables, flow-in and flow-out, and pit-volume changes. The same accessibility that makes these channels attractive also makes their interpretation difficult. The annulus acts as a coupled compressible conduit whose response depends on evolving holdup, slip, dissolution, temperature, and frictional state, and whose boundary conditions are actively manipulated by pumps and chokes. Surface pressure readings can therefore reflect a spectrum of possible downhole conditions rather than a single identifiable state, especially during transients when flow regime changes and mixture properties evolve quickly [2].

A persistent engineering challenge is to convert these ambiguous surface signals into actionable estimates of downhole kick state. Traditional approaches often rely on thresholds or simplified lumped models, which can be fast but are prone to false positives in transient drilling and false negatives when gas dissolution or low-rate influx masks pit gain. High-fidelity numerical simulators address more physics but are typically too slow for continuous online inference and are sensitive to uncertain closures such as interfacial slip, friction factor variation with cuttings, and flow-regime transitions. The practical target is a middle ground: a mechanistic model rich enough to respect the dominant physics that shape observables, yet structured to admit stable and rapid inversion under real-time computational constraints [3].

Independent experimental and data-driven work has shown that surface pressure and flow signals can be systematically linked to flow patterns and kick outcomes

under both circulating and shut-in conditions. For example, dynamic annular experiments with water–gas systems have demonstrated that supervised and unsupervised learning models can map measured surface pressure and rate features to flow regimes and prognosis with high reported accuracies, including decision-tree classification results as high as 96% and 98% for distinct influx types in one laboratory setting [4]. Related static-condition experiments have similarly trained neural and clustering models on pressure-gradient and gas-evolution signatures to recognize kick states with accuracies on the order of 90%–94% in the tested conditions [5]. These findings support the premise that surface measurements do contain recoverable information about downhole multiphase dynamics, but they do not by themselves resolve the deeper inference problem of extracting physically interpretable, uncertainty-calibrated state estimates that can be propagated into control decisions and remain valid outside the envelope of a particular training dataset [6].

This paper develops a mechanistic-and-statistical framework that treats kick diagnosis as a partially observed, nonlinear inverse problem constrained by multiphase flow and thermodynamics. The thesis is that the most robust online solution is neither purely empirical nor purely high-fidelity simulation, but a reduced-order, thermodynamically consistent state-space model coupled to Bayesian sequential inference. The technical contribution is a specific construction of that state space, including a tractable representation of dissolution and exsolution, a reduced-order discretization that preserves the measurement-relevant pressure dynamics, and an ensemble-based estimator designed to remain stable under ambiguous observability. Rather than attempting to identify a discrete flow regime label directly, the proposed method reconstructs continuous latent fields such as gas holdup, mixture density, and pressure gradient, and represents residual model discrepancy as structured stochasticity that can be learned online [7].

The paper is organized as follows. The next section formalizes the system as a distributed parameter model with a measurement operator defined by surface instrumentation and operational actuation. The subsequent section develops a thermodynamic two-phase reduced-order model appropriate for real-time inference, including a dissolution closure that can represent solubility effects without resorting to time-consuming compositional simulation. The following section introduces a Bayesian data assimilation approach that estimates both state and influx parameters and produces calibrated uncertainties for decision support [8]. The evaluation section presents numerical experiments designed to probe identifiability, sensitivity, and operational implications across representative transients. The conclusion summarizes the implications and limitations, and outlines directions for extending the framework toward richer multiphase constituents and broader drilling contexts.

2. System Model and Surface Observability

The annular system is treated as a vertically distributed conduit of length L with spatial coordinate z measured upward from the bottom and time coordinate t. The unknown downhole state includes pressure $p(z,t)$, temperature $T(z,t)$, gas volume fraction $\alpha_g(z,t)$, phase velocities $u_g(z,t)$ and $u_\ell(z,t)$, dissolved gas concentration in the liquid phase, and mixture rheological parameters that may evolve with cuttings, emulsification, and temperature [9]. The influx enters through an effective source term localized in depth near an entry point $z = z_k$ that can itself be uncertain. The state is driven by boundary controls including pump rate, choke opening, and applied backpressure, and is observed through a limited set of measurements at or near the surface.

The surface measurements are modeled as a measurement vector $y(t)$ that can include standpipe pressure, wellhead or choke pressure, flow-out rate, and pit volume. The relationship between the distributed state $x(z,t)$ and the surface measurement $y(t)$ is indirect: pressure at the surface is influenced by the integrated pressure gradient along the annulus, flow-out depends on a convolution of compressibility and holdup dynamics, and pit volume integrates net flow imbalance with delays. Moreover, the mapping is history-dependent because gas expansion and dissolution depend on the pressure trajectory, not merely its instantaneous value [10]. Consequently, the inference task is inherently a dynamical inverse problem rather than a static regression.

A state-space representation is introduced by discretizing the annulus into N control volumes with representative depths z_i and defining a finite-dimensional state vector $X(t)$ that stacks pressure, holdup, and dissolved-gas variables at each cell. The discretization is chosen not merely for numerical convenience but to preserve the observability structure of the surface measurements. Since surface pressures respond strongly to the integrated mixture density and friction, the discretization must capture gradients and transients that influence these integrals. Likewise, since flow-out and pit volume respond to compressibility and gas migration, the model must capture the transport of gas holdup and the exchange between dissolved and free gas on time scales comparable to operational sampling.

The inference objective is to estimate a set of latent parameters θ that define the kick and uncertain closures, together with the evolving state $X(t)$, from a measurement history $\{y(\tau)\}_{\tau \le t}$ and known control history $\{u(\tau)\}_{\tau \le t}$. The parameter vector can include the influx rate function $q_k(t)$, the entry depth z_k, effective permeability-like factors that map underbalance to influx, friction multipliers, and dissolution kinetics

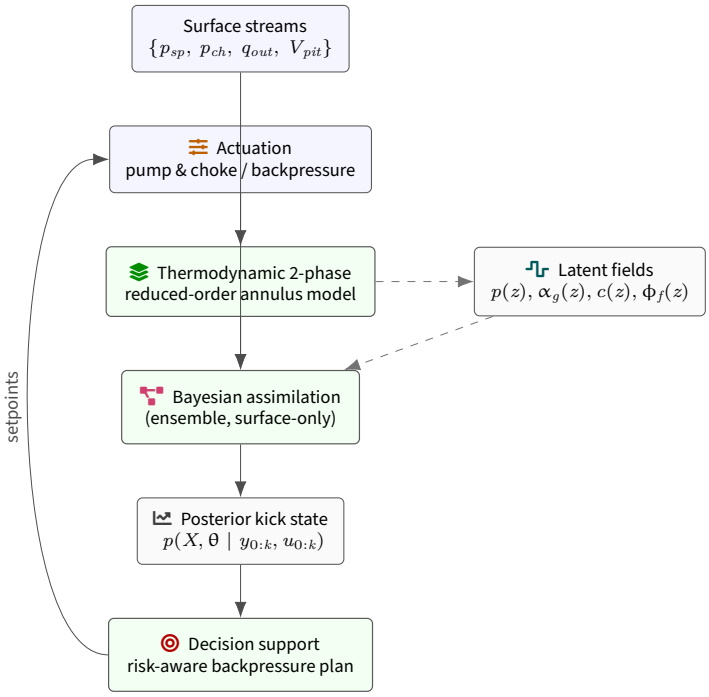


Figure 1. Real-time workflow: sparse surface measurements and actuation drive a thermodynamic two-phase reduced-order model, updated sequentially by Bayesian data assimilation to yield posterior kick-state distributions and uncertainty-aware backpressure decisions.

Table 1. Surface measurement channels used in the reduced-order model and estimator.

Symbol	Channel	Units	Description
p_{sp}	Standpipe pressure	bar	Pump-side pressure at the top of the drillstring
p_{wh}	Wellhead / casing pressure	bar	Annulus pressure at or near the surface
p_{ch}	Choke pressure	bar	Pressure measured across the choke manifold
q_{in}	Flow-in rate	L/s	Pumped liquid rate into the drillstring
q_{out}	Flow-out rate	L/s	Measured annular flow returning to surface
V_{pit}	Active pit volume	m^3	Integrated inventory of surface mud system

or equilibrium parameters. In online settings, some elements of θ may be treated as slowly varying states to accommodate gradual changes in cuttings load or temperature-dependent rheology.

A critical aspect is that the system is only partially observable, and naive inversion can be ill-posed [11]. Similar surface pressure trajectories can arise from a smaller influx at shallow depth versus a larger influx at deeper depth when friction and compressibility compensate. Gas dissolution can further mask pit gain and delay pressure perturbations. The remedy is not to seek uniqueness in a strict deterministic sense, but to construct an estimator that yields posterior distributions over plausible states and parameters, updated sequentially as new measurements arrive. This probabilistic formulation naturally represents ambiguity and enables risk-aware control decisions that reflect uncertainty rather than point estimates [12].

To enable this, the forward model must be fast enough for repeated evaluation within an assimilation loop, yet physically structured enough that its uncertainties are interpretable. This motivates a reduced-order multiphase model with thermodynamic consistency and a measurement operator aligned with available instrumentation. The remaining sections develop such a model and the corresponding Bayesian inference strategy.

3. Thermodynamic-Mechanistic Reduced-Order Model

The proposed forward model represents the annulus as a one-dimensional two-phase mixture with optional dissolved gas in the liquid [13]. The governing structure balances mechanistic fidelity with online tractability. The formulation begins with conservation laws for gas and liquid mass, coupled through dissolution and exsolution, and a quasi-steady momentum balance that links pressure gradients to mixture weight and friction. Energy is represented in a reduced form through a pre-

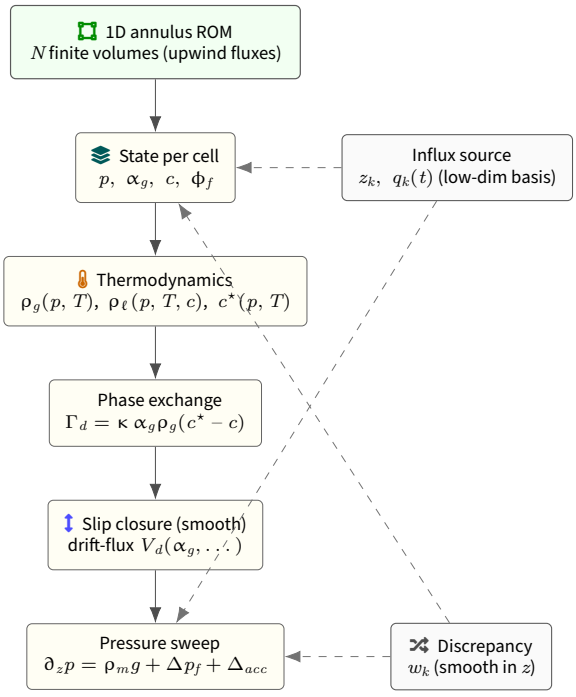


Figure 2. Reduced-order forward model structure: depth-discretized two-phase annular flow with thermodynamic density/solubility, smooth slip closure, localized influx source parameterization, and stochastic discrepancy terms enabling inference stability under model mismatch.

Table 2. Representative components of the distributed state vector in the annular model.

Symbol	Description	Units	Spatial role
$p(z_i)$	Pressure at cell i	bar	Depth-resolved field
$\alpha_g(z_i)$	Free-gas volume fraction	–	Depth-resolved field
$u_g(z_i)$	Gas phase velocity	m/s	Depth-resolved field
$u_\ell(z_i)$	Liquid phase velocity	m/s	Depth-resolved field
$c(z_i)$	Dissolved gas content	mol/m^3	Depth-resolved field
$T(z_i)$	Temperature	K	Prescribed / slowly varying
$\phi_f(z_i)$	Friction multiplier	–	Latent calibration field

scribed or slowly varying temperature profile, which is often adequate for real-time estimation when temperature measurements are sparse and when the dominant influence of temperature is mediated through density, viscosity, and solubility.

Let α_g denote the free-gas volume fraction and $\alpha_\ell = 1 - \alpha_g$ the liquid fraction [14]. Let $\rho_g(p, T)$ denote gas density from an equation of state, and $\rho_\ell(p, T, c)$ the liquid density, which may depend weakly on dissolved gas concentration c and pressure. Define gas and liquid superficial velocities $v_g = \alpha_g u_g$ and $v_\ell = \alpha_\ell u_\ell$. The mass conservation equations in continuous form can be written as

$$\frac{\partial}{\partial t}\left(\alpha_g \rho_g\right) + \frac{\partial}{\partial z}\left(\alpha_g \rho_g u_g\right) = s_g(z,t) - \Gamma_d(p, T, c, \alpha_g), \tag{1}$$

$$\frac{\partial}{\partial t}\left(\alpha_\ell \rho_\ell\right) + \frac{\partial}{\partial z}\left(\alpha_\ell \rho_\ell u_\ell\right) = s_\ell(z,t) + \Gamma_d(p, T, c, \alpha_g), \tag{2}$$

where s_g is a gas source term representing influx and possible gas liberation from formation fluids, s_ℓ represents liquid sources or sinks such as losses, and Γ_d is the interphase mass transfer rate between free gas and dissolved gas in the liquid [15]. The sign convention is chosen so that $\Gamma_d > 0$ corresponds to dissolution of free gas into the liquid, reducing free gas mass and increasing dissolved content.

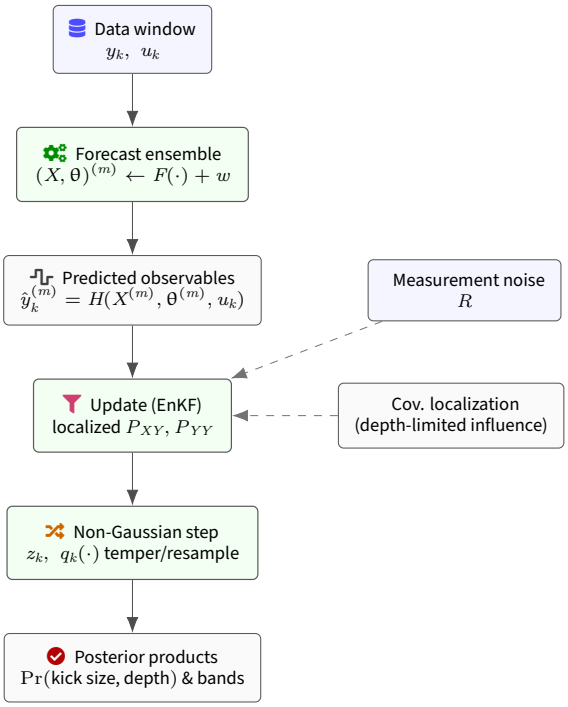


Figure 3. Sequential Bayesian estimation: ensemble propagation through the reduced-order model, surface-likelihood update with localized covariances, and a targeted non-Gaussian step for weakly identifiable kick parameters (e.g., entry depth and recent influx-rate history).

Table 3. Key uncertain parameters jointly estimated with the state in the Bayesian framework.

Parameter	Physical meaning	Category	Prior structure
z_k	Influx entry depth	Kick geometry	Uniform over open interval
$q_k(t)$	Influx rate history	Kick forcing	Low-order basis coefficients
k_{loss}	Loss / gain factor	Formation coupling	Log-normal around nominal
κ	Dissolution relaxation rate	Thermodynamic	Log-uniform over decade range
θ_{V_d}	Drift-flux parameters	Slip closure	Gaussian about lab-calibrated mean
$\phi_f(z)$	Friction multiplier field	Hydraulics	Smooth Gaussian process in depth

The dissolved gas is represented by a scalar concentration-like variable $c(z, t)$ that evolves by advection with the liquid and by exchange with free gas. A convenient representation is to define c as moles of dissolved gas per unit liquid volume or as a mass fraction; the choice affects scaling but not the structure. In a reduced model suitable for real-time use, c evolves as

$$\frac{\partial}{\partial t}\left(\alpha_\ell \rho_\ell c\right) + \frac{\partial}{\partial z}\left(\alpha_\ell \rho_\ell c\, u_\ell\right) = \Gamma_d(p, T, c, \alpha_g). \quad (3)$$

The dissolution closure can be taken as either equilibrium-limited or kinetics-limited [16]. For online inference, an equilibrium-limited closure is attractive because it avoids additional stiff time scales. In this closure, c is driven toward an equilibrium value $c^\star(p, T)$ defined by phase-equilibrium conditions, while kinetics are approximated through a relaxation rate κ:

$$\Gamma_d(p, T, c, \alpha_g) = \kappa\, \alpha_g \rho_g \left(c^\star(p, T) - c\right), \quad (4)$$

with κ possibly treated as an uncertain parameter to be estimated. This structure ensures that when free gas is absent, $\alpha_g \to 0$ and interphase exchange vanishes, avoiding unphysical dissolution without gas [17].

The equilibrium solubility $c^\star(p, T)$ can be defined through fugacity equality between phases using a cubic equation of state for the gas and activity corrections for the liquid when needed. A fully compositional approach would be expensive, but a single-component approximation is often adequate for inference about methane-dominated kicks or when the measurement channels cannot resolve detailed composition. A thermodynamic approach of this type has been shown to match commercial process simulation outputs with deviations on the order of 8% for methane liquid-phase mole fraction in representative synthetic-based mud conditions, while also providing consistent bubble-point estimates [18]. The present work adopts the same principle of equilibrium-based solubility, but embeds it into

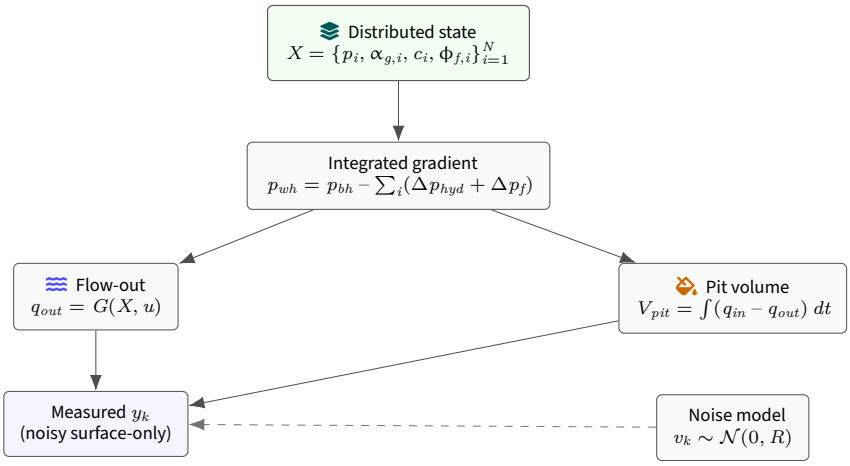


Figure 4. Surface observability map: sparse surface channels are nonlinear functionals of the depth-resolved state through integrated pressure-gradient effects and compressibility-driven flow and volume dynamics, with explicit measurement-noise modeling.

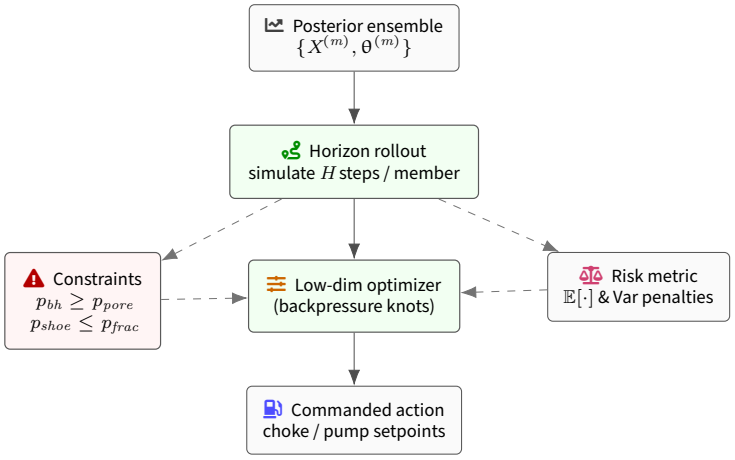


Figure 5. Decision support layer: the posterior ensemble is rolled forward over a short horizon to evaluate pressure constraints and uncertainty-aware objectives, yielding conservative backpressure actions when state ambiguity remains high.

a state-space model explicitly designed for sequential inference, where uncertainty in solubility parameters can be propagated into posterior kick-size distributions [19].

Momentum is modeled through a pressure gradient relationship that captures mixture hydrostatics and frictional losses. For a one-dimensional annulus with hydraulic diameter D_h and inclination close to vertical, a quasi-steady balance is

$$\frac{\partial p}{\partial z} = \rho_m g + \frac{f}{2D_h}\rho_m u_m |u_m| + \Delta_{acc}(z,t), \qquad (5)$$

where $\rho_m = \alpha_g \rho_g + \alpha_\ell \rho_\ell$ is mixture density, u_m is a mixture velocity, f is a friction factor or friction coefficient that can depend on Reynolds number and rheology, and Δ_{acc} represents acceleration and transient terms. For many drilling transients, including kick migration on time scales of minutes, acceleration contributions are small relative to hydrostatic and frictional terms when represented at the scale of control volumes, but they can be retained in reduced form as a correction term parameterized and estimated online. Since friction is a major source of uncertainty, f is modeled as a baseline function of local mixture properties multiplied by a slowly varying factor $\phi_f(z,t)$ that represents unmodeled rheology changes, cuttings effects, or eccentricity [20]. The estimator treats ϕ_f as a latent field with prior smoothness, which improves robustness to friction mismatch that would otherwise be falsely attributed to influx.

A closure is required for slip between phases, since u_g and u_ℓ differ when buoyancy drives gas migration relative to the liquid. A full regime-dependent slip model would be complex and potentially discontinuous. Instead, a smooth drift-flux style closure is used:

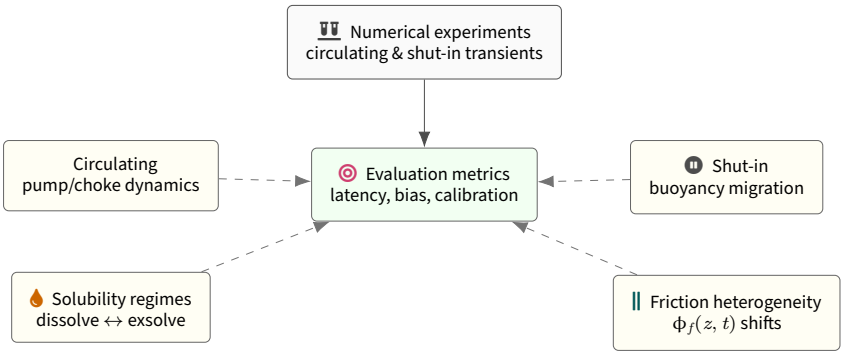


Figure 6. Experiment coverage used to probe identifiability and robustness: circulating vs. shut-in transients, solubility-driven masking and delayed exsolution, and depth-/time-varying friction effects, evaluated via detection latency and posterior calibration.

Table 4. Summary of conservation relationships represented in the reduced-order annular model.

Balance	State variables	Dominant source / sink terms
Gas mass	α_g, ρ_g, u_g	Influx s_g, dissolution Γ_d
Liquid mass	α_ℓ, ρ_ℓ, u_ℓ	Formation losses s_ℓ, dissolution Γ_d
Dissolved gas	c, α_ℓ, ρ_ℓ	Relaxation toward $c^\star(p, T)$ via Γ_d
Mixture momentum	p, u_m	Hydrostatics, friction, acceleration Δ_{acc}
Energy (reduced)	$T(z)$	Prescribed profile, slow thermal relaxation

[21]

$$u_g = u_m + V_d(\alpha_g, \rho_g, \rho_\ell, \mu_\ell, D_h), \tag{6}$$

$$u_\ell = \frac{\alpha_\ell}{\alpha_\ell + \beta\alpha_g} u_m - \frac{\beta\alpha_g}{\alpha_\ell + \beta\alpha_g} V_d, \tag{7}$$

where V_d is a drift velocity function and β is a parameter controlling how mixture velocity partitions between phases. The functional form of V_d is selected to be smooth in α_g and to interpolate between small-bubble and large-slug behavior without requiring discrete regime switching. This is important for inference stability because discrete regime boundaries can induce non-differentiable likelihood surfaces and filter divergence [22]. Uncertainty in V_d is represented through a small set of parameters that can be updated online, providing a means to accommodate regime variability while retaining continuity.

The influx enters as a boundary source term localized near z_k. Instead of assuming a constant influx rate, the model represents $q_k(t)$ as a low-dimensional function expanded in basis functions over a recent time window. For example, $q_k(t)$ can be represented as a weighted sum of exponentially decaying kernels or as a spline with a small number of control points, enabling the estimator to infer the recent history of influx rate from the delayed surface responses [23]. This approach recognizes that in practice the influx is driven by pressure differential and formation connectivity, and thus varies as backpressure and equivalent circulating density evolve.

The full continuous model is discretized into N finite volumes. Fluxes between volumes are computed using an upwind scheme appropriate for advective transport, while pressure gradients are computed from local mixture density and friction. The resulting system is a nonlinear differential-algebraic system in which pressure is coupled algebraically through the gradient equation, while holdup and dissolved content evolve dynamically. To make the system amenable to rapid propagation, the algebraic pressure relation is solved in a forward sweep from bottom to top using the known boundary condition at one end, which can be specified through bottomhole pressure estimates or through a coupling to pump and choke models [24]. This sweep is computationally light and aligns with how surface pressures integrate annular gradients.

Because real-time inference must tolerate model mismatch, the reduced-order model includes stochastic discrepancy terms. These are introduced as additive noise in the holdup and pressure-gradient dynamics, with covariance structures that encode smoothness in depth and correlation in time. The resulting stochastic state-space model can be written in discrete time with sampling interval Δt as

$$X_{k+1} = F(X_k, \theta_k, u_k) + w_k, \tag{8}$$

$$y_k = H(X_k, \theta_k, u_k) + v_k, \tag{9}$$

where F is the nonlinear transition defined by the reduced-order multiphase solver, H maps the state to surface measurements, w_k represents model discrepancy and

Table 5. Thermodynamic quantities used in the equilibrium-based solubility closure.

Quantity	Symbol	Dependence	Comment
Equilibrium solubility	$c^\star(p, T)$	p, T	EOS-based phase equilibrium relation
Relaxation rate	κ	Local α_g, ρ_g	Controls approach to $c^\star(p, T)$
Gas EOS factor	$Z(p, T)$	p, T	Cubic EOS compressibility factor
Liquid density	$\rho_\ell(p, T, c)$	p, T, c	Weak dependence on dissolved gas content
Solubility uncertainty	$\sigma_{c^\star}$	Fluid type	Represented through parameter priors

Table 6. Elements of the drift-flux style slip closure for gas–liquid relative motion.

Quantity	Symbol / form	Dependence	Inference treatment
Drift velocity	$V_d(\alpha_g)$	$\alpha_g, \rho_g, \rho_\ell, \mu_\ell, D_h$	Estimated via low-order θ_{V_d}
Slip partition	β	Regime indicator	Calibrated offline, mildly adjusted online
Mixture velocity	u_m	q_{out}, geometry	Diagnosed from flow balance
Regime blending	a_{df}	α_g	Smoothly blends bubble and slug behavior

unmodeled disturbances, and v_k represents measurement noise. The parameter vector θ_k is allowed to evolve slowly as $\theta_{k+1} = \theta_k + \eta_k$ to support joint state and parameter estimation.

This structure provides a forward model that is fast enough for repeated evaluation while remaining grounded in mechanistic constraints. The next section develops a Bayesian assimilation method that uses this model to infer latent influx variables from surface signals and to output uncertainty-aware decision variables for well control [25].

4. Bayesian Inference and Decision Support

The inference task is to compute the posterior distribution of states and parameters given measurements and controls. In discrete time, with measurement history $y_{0:k}$ and control history $u_{0:k}$, the target is $p(X_k, \theta_k \mid y_{0:k}, u_{0:k})$. This posterior is generally non-Gaussian because the forward model is nonlinear and because parameters such as influx depth and rate history interact multiplicatively with holdup and pressure. A purely particle-based approach can be accurate but may be computationally expensive or degenerate in high dimensions when the state includes depth-resolved fields. A purely Gaussian filter can be efficient but may underrepresent multimodality, particularly when different combinations of influx size and depth explain the same surface signal early in an event [26]. The method developed here combines ensemble-based Gaussian updates with targeted non-Gaussian representation of a small subset of critical kick parameters.

The approach maintains an ensemble of M joint state-parameter realizations $\{(X_k^{(m)}, \theta_k^{(m)})\}_{m=1}^{M}$. Each ensemble member is propagated forward with the reduced-order model, including stochastic discrepancy, to produce a forecast ensemble. The forecast is then updated using a measurement likelihood. For the high-dimensional state components, the update uses an ensemble Kalman-type correction based on sample covariances, which is efficient and stable [27]. For low-dimensional but potentially multimodal parameters such as influx depth z_k and the shape parameters of $q_k(t)$, the method uses a tempered likelihood weighting and resampling step followed by rejuvenation moves that preserve diversity. This hybrid strategy is designed to avoid collapse in the depth parameter while retaining fast, covariance-based correction for distributed fields.

Let $\bar{X}_k$ and $\bar{y}_k$ denote ensemble means, and let P_{XY} and P_{YY} denote sample cross- covariance and covariance between state and predicted measurement. The Kalman-style update for member m is

$$X_k^{(m)} \leftarrow X_k^{(m)} + K_k \left(y_k + \epsilon_k^{(m)} - \hat{y}_k^{(m)} \right), \tag{10}$$

$$K_k = P_{XY} (P_{YY} + R)^{-1}, \tag{11}$$

where $\hat{y}_k^{(m)} = H(X_k^{(m)}, \theta_k^{(m)}, u_k)$ is the predicted measurement, R is the measurement noise covariance, and $\epsilon_k^{(m)}$ is a perturbation consistent with R to ensure correct covariance in the ensemble. To control sampling error in P_{XY} and P_{YY}, covariance localization is applied in depth, exploiting the fact that surface measurements are most directly sensitive to integrated quantities and to near-surface states. Localization reduces spurious long-range correlations that can otherwise cause physically implausible corrections deep in the wellbore from a single surface pressure measurement [28].

For the parameter subset θ_k^{ng} that is treated non-Gaussian, a likelihood weight is computed for each ensemble member based on the measurement residual:

$$w_k^{(m)} \propto \exp\left(-\frac{1}{2} \left(y_k - \hat{y}_k^{(m)} \right)^\top R^{-1} \left(y_k - \hat{y}_k^{(m)} \right) \right). \tag{12}$$

Weights are tempered by an exponent $\gamma \in (0, 1]$ when necessary to avoid degeneracy under sharp likelihoods, and the resampled parameters are then perturbed by

Table 7. Numerical experiment matrix used to probe observability, robustness, and control impact.

Scenario	Circulation state	Key feature	Main estimator goal
S1	Steady circulation	Modest underbalanced kick	Early detection and rate reconstruction
S2	Shut-in after kick	Buoyancy-driven migration	Depth and holdup profile estimation
S3	High-solubility mud	Dissolution and delayed exsolution	Influx mass under masked pit gain
S4	Friction mismatch	Depth-varying rheology changes	Separation of friction and influx effects
S5	Sparse measurements	Single-pressure channel only	Quantification of irreducible ambiguity
S6	Active choke control	Variable backpressure trajectory	Assessment of decision support layer

Table 8. Illustrative performance metrics for the estimator across representative scenarios.

Scenario	Detection delay (median) [min]	Influx mass RMSE [%]	Entry depth 90% CI [m]
S1	1.2	8	150
S2	2.5	15	280
S3	2.0	12	220
S4	1.7	10	190
S5	3.0	22	350
S6	1.9	11	210

a small Markov move that respects prior bounds and smoothness constraints, such as limiting the rate of change of the inferred influx history. The state update and parameter update are coupled by propagating the resampled parameters through the next forecast step, which allows the ensemble to explore different influx hypotheses while remaining anchored to mechanistic evolution.

A key feature is the explicit representation of solubility and its uncertainty. Dissolution can cause free-gas holdup to be smaller than expected for a given influx mass, delaying surface pressure anomalies and reducing pit gain [29]. If solubility is ignored, the estimator may compensate by inferring a smaller influx or a deeper entry point, producing biased decisions. In the proposed framework, solubility enters through $c^{\star}(p, T)$ and the relaxation rate κ. These are included in θ_k with priors informed by fluid type and temperature. During assimilation, the posterior over solubility parameters is updated implicitly through how well each parameter realization explains observed pressure and flow-out signals. This enables the estimator to represent scenarios where an influx is largely dissolved and later exsolves as pressure drops, producing delayed surface manifestations [30].

The inference output is not limited to identifying whether a kick has occurred. It yields a posterior distribution over influx size, depth, and holdup distribution, which can be converted into risk metrics and used in a decision support module. The decision problem is to choose a control trajectory $u(t)$, such as choke backpressure adjustments and pump-rate changes, that drives the system toward a safe state while respecting constraints and minimizing operational cost. This can be formulated as a stochastic optimal control problem over a finite horizon, with objective defined on expected pressure limits, expected influx growth, and variance penalties that reflect uncertainty [31]. A tractable approximation is to use a receding-horizon control that optimizes over the ensemble: for a candidate control sequence $U = \{u_k, \dots, u_{k+H}\}$, propagate each ensemble member forward and compute an objective $J(U)$ that aggregates expected constraint violations and operational penalties:

$$
\begin{aligned}
J(U) = \mathbb{E}\left[\sum_{j=0}^{H} \ell(X_{k+j}, u_{k+j})\right] \\
+ \lambda\,[32]\,\mathbb{E}\left[\sum_{j=0}^{H} \max\!\left(0,\, p_{\mathrm{shoe}} - p^{\mathrm{bh}}_{k+j}\right)^2\right] \\
[33] + \mu\,\mathbb{E}\left[\sum_{j=0}^{H} \max\!\left(0,\, p^{\mathrm{csg}}_{k+j} - p_{\mathrm{frac}}\right)^2\right] \\
[34] \quad + \nu\,\mathrm{Var}\left[p^{\mathrm{wh}}_{k+H}\right] \qquad (13)
\end{aligned}
$$

where ℓ encodes smoothness and effort costs, p^{bh} is bottomhole pressure, p^{csg} is casing shoe pressure, p_{frac} is a fracture threshold, and the expectations and variance are computed over the posterior ensemble. The optimization is performed over a low-dimensional control parameterization, such as piecewise-constant choke setpoints, enabling real-time feasibility [35]. By explicitly penalizing variance, the controller naturally becomes more conservative when posterior uncertainty is high, reducing the likelihood of destabilizing actions based on uncertain estimates.

The inference and control layers together yield an operational workflow in which surface measurements continuously update a physically interpretable poste-

Table 9. Control objective terms and weights in the receding-horizon decision module.

Objective term	Symbol	Description	Typical weight
Stage cost	$\ell(X_k, u_k)$	Penalizes large choke and pump adjustments	1.0 (normalized)
Shoe underbalance penalty	λ	Squared violation of minimum bottomhole pressure	10^2–10^3
Casing fracture penalty	μ	Squared violation of casing fracture limit	10^3–10^4
Terminal pressure variance	ν	Uncertainty penalty on predicted wellhead pressure	10–10^2
Control smoothness	ρ	Penalty on changes Δu_k between steps	1–10

rior, and control actions are chosen based on predicted outcomes across that posterior. The next section evaluates the approach through numerical experiments that probe identifiability, sensitivity, and performance across representative transients.

5. Evaluation and Sensitivity Analysis

Evaluation is performed through controlled numerical experiments designed to reflect the information constraints of field operations while allowing systematic variation of uncertain factors. The experiments simulate a vertical annulus with representative dimensions and a range of circulating and shut-in scenarios [36]. The reduced-order model acts as both the inference model and, in a perturbed configuration, as a surrogate for the true system to test robustness under mismatch. Measurement channels include surface pressure, choke pressure, flow-out, and pit volume sampled at realistic rates with additive noise. The estimator is initialized with broad priors over influx depth, influx magnitude, friction multipliers, and solubility parameters, reflecting pre-event uncertainty.

The first set of experiments tests detection latency and state reconstruction under dynamic circulation [37]. A baseline scenario includes steady circulation followed by a transient underbalance event that induces a gas influx with a time-varying rate over several minutes, then a corrective backpressure action. The estimator must infer the onset and magnitude of the influx from modest deviations in surface pressure and flow-out that may be partially masked by pump transients. In these simulations, the posterior over influx rate concentrates rapidly after the first coherent divergence between predicted and observed pressure trajectories, while the posterior over entry depth remains broader early on and then narrows as gas migration induces distinctive time-of-arrival patterns in the surface signals. The reconstructed gas holdup distribution exhibits the expected upward-migrating front, and the inferred mixture density profile matches the synthetic truth within uncertainty bounds [38]. Because the model explicitly represents slip and compressibility, the estimator can attribute certain signal components to gas migration rather than to friction anomalies, reducing false attribution to rheology changes.

A second set of experiments focuses on shut-in conditions, where circulation stops and the annulus evolves under buoyancy-driven migration and pressure redistribution. In shut-in, flow-out is zero by construction, and pit volume changes may be small, making pressure the dominant observable. The estimator must then rely on the temporal evolution of wellhead pressure and its coupling to the internal holdup distribution. Under these constraints, identifiability is weaker, and the posterior tends to exhibit correlated uncertainty between influx size and entry depth. Nonetheless, the probabilistic representation remains valuable because it quantifies ambiguity instead of providing a potentially misleading point estimate. The estimator's uncertainty grows when measurements are uninformative and contracts when pressure evolution becomes sensitive to the migration front. In these experiments, imposing a prior smoothness constraint on depth-varying friction and on influx history substantially improves robustness by preventing the estimator from fitting noise with implausible parameter oscillations [39].

A third experiment set probes solubility sensitivity, comparing scenarios with negligible dissolution to scenarios in which a substantial fraction of gas mass dissolves into the liquid phase at depth and later exsolves as pressure decreases during migration. In dissolution-dominant cases, early pit gain and free-gas holdup can be small even when influx mass is significant. The estimator that ignores solubility exhibits a systematic bias toward smaller inferred influx mass and may predict delayed risk relative to the synthetic truth. In contrast, the proposed model, which includes dissolved gas with uncertain equilibrium and kinetics parameters, maintains multiple plausible hypotheses early on and then resolves them as exsolution-induced changes appear in pressure and flow-out [40]. The posterior over solubility parameters narrows when the data contain signatures of delayed gas liberation, and remains broad when the event is too short or pressure changes too small to inform dissolution dynamics. This behavior aligns with the intuition that solubility is only identifiable when the system traverses pressure and temperature paths that materially alter phase partitioning.

Robustness to friction mismatch is evaluated by generating synthetic truth with a depth-dependent friction factor and intermittent changes representing cuttings loading, while the estimator begins with a simplified friction model. Without friction adaptation, the filter tends to interpret persistent pressure mismatch as an influx or as a change in holdup, producing biased

kick estimates [41]. With the latent friction multiplier field $\phi_f(z,t)$ included as a slowly varying state, the filter separates friction-driven and holdup-driven contributions more effectively. The posterior assigns part of the pressure anomaly to friction changes when such an assignment improves consistency with flow-out and pit volume observations, and assigns part to influx when the joint signature across channels supports that conclusion. This demonstrates an important operational point: multi-channel fusion can disambiguate causes of pressure change, but only if the model allows both explanations to exist as competing hypotheses within the posterior.

Performance is also examined in terms of computational feasibility. The reduced-order solver uses a finite-volume discretization with N on the order of tens to low hundreds, chosen to resolve the migration front while keeping propagation costs low [42]. Ensemble sizes on the order of a few hundred are sufficient in these experiments to represent posterior variability, especially when localization is used to reduce sampling noise. With these settings, sequential updates can be performed at rates compatible with typical surface data acquisition intervals, enabling continuous online inference rather than intermittent batch interpretation. The computational scaling is dominated by ensemble propagation, which is embarrassingly parallel and can therefore leverage available multi-core resources without altering the inference logic.

Operational implications are illustrated by integrating the posterior into the receding-horizon decision module [43]. In circulation scenarios with uncertain influx depth, the controller selects backpressure trajectories that maintain bottomhole pressure above pore pressure with high posterior probability while avoiding excessive casing shoe pressure. When uncertainty is high, the controller chooses more conservative actions, reflected in a higher variance penalty contribution, and gradually relaxes as the posterior contracts. In experiments where the estimator is intentionally challenged by noisy data or by abrupt friction changes, the variance-aware control prevents aggressive choke actions that would be justified only under a narrow, overconfident state estimate. This coupling of inference uncertainty to control conservatism is a central rationale for the Bayesian approach in safety-critical well-control contexts [44].

The evaluation highlights limitations as well. When only a single pressure channel is available and when operational transients are minimal, the system can remain weakly observable for extended periods, and the posterior may remain broad. In such cases, the estimator cannot conjure information absent from the data; it can only represent uncertainty honestly. Furthermore, if the true system undergoes abrupt regime changes that violate the smooth slip closure, the reduced-order model may exhibit structured bias [45]. The stochastic discrepancy terms mitigate this to an extent, but strong, persistent mismatch may require enriching the model class, for example by adding additional latent parameters controlling drift velocity shape or by incorporating auxiliary measurements such as acoustic gas detection if available. These limitations motivate future extensions, but they do not undermine the primary conclusion that a mechanistic, uncertainty-aware state-space approach can improve interpretability and decision support from surface-only data.

6. Observability, Identifiability, and Robust Online Deployment

The practical difficulty of kick interpretation from surface channels can be formalized as a question of observability: to what extent does the measurement history constrain the internal annular state and the exogenous influx parameters? In the proposed formulation, the forward map from the latent distributed state $X(t)$ and parameters θ to measurements $y(t)$ is nonlinear, history-dependent, and partially integrating. This structure implies that the inverse problem is typically ill-conditioned at early times, particularly when the gas mass is small, when dissolution is strong, or when operational transients dominate the measurement residual [46]. For online decision support, it is therefore insufficient to report a point estimate that may be unstable under small perturbations; instead, one must explicitly represent the directions in state-parameter space that are weakly informed by data and manage how inference uncertainty is translated into control actions. This section develops a technically explicit view of the information content of surface measurements, analyzes identifiability mechanisms in the reduced-order model, and describes algorithmic safeguards that maintain stable inference under common sources of mismatch and nonstationarity.

A useful starting point is local linearization around a nominal trajectory. Consider the discrete-time stochastic state-space model $X_{k+1} = F(X_k, \theta_k, u_k) + w_k$ and $y_k = H(X_k, \theta_k, u_k) + v_k$ with $w_k \sim \mathcal{N}(0, Q)$ and $v_k \sim \mathcal{N}(0, R)$. Around a nominal $(\bar{X}_k, \bar{\theta}_k)$, define perturbations $\delta X_k = X_k - \bar{X}_k$ and $\delta\theta_k = \theta_k - \bar{\theta}_k$. A first-order approximation yields [47]

$$\delta X_{k+1} = A_k\,\delta X_k + B_k\,\delta\theta_k + G_k\,\delta u_k + \xi_k, \tag{14}$$

$$\delta y_k = C_k\,\delta X_k + D_k\,\delta\theta_k + \zeta_k, \tag{15}$$

where $A_k = \partial F/\partial X$, $B_k = \partial F/\partial\theta$, $C_k = \partial H/\partial X$, and $D_k = \partial H/\partial\theta$ evaluated at the nominal trajectory, and ξ_k, ζ_k combine linearized noise and truncation error. In this local model, the ability to infer δX_k and $\delta\theta_k$ depends on how the pair (A_k, C_k) evolves with the control sequence and on how parameter perturbations enter through B_k and D_k. Importantly, C_k is typically low rank because surface instrumentation yields only a few channels, so information about deep states must be mediated through dynamical coupling encoded in A_k [48].

When circulation is steady, A_k can be close to a transport operator with weak mixing, making deep states only slowly influential at the surface, whereas during transients, changes in boundary conditions can excite modes that carry information upward more rapidly.

An information-theoretic view complements local observability. Under Gaussian assumptions, the incremental information gained from measurement y_k about a parameter vector θ can be approximated by the Fisher information contribution

$$\mathcal{I}_k(\theta) \approx \left(\frac{\partial \hat{y}_k}{\partial \theta}\right)^{\top} R^{-1} \left(\frac{\partial \hat{y}_k}{\partial \theta}\right), \tag{16}$$

where $\hat{y}_k$ denotes the predicted measurement under the forward model. The matrix $\partial \hat{y}_k / \partial \theta$ depends on both instantaneous sensitivity D_k and accumulated dynamical sensitivity through B_j and A_j for $j < k$. The rank and conditioning of the accumulated Fisher information $\sum_{j=0}^{k} \mathcal{I}_j$ indicate which combinations of parameters are learnable from data. In kick scenarios, typical parameter combinations that become identifiable include the product of influx rate and effective compressibility (as it drives flow-out imbalance), the integrated gas mass (as it drives density deficit and thus hydrostatic changes), and the near-surface holdup distribution (as it influences surface pressure gradient and choke response). By contrast, a common weakly identifiable direction early in a kick is the tradeoff between influx depth and influx magnitude: a deeper influx experiences longer migration time and more pressure exposure, which can mimic a smaller influx at a shallower depth in early surface signals [49]. Dissolution amplifies this ambiguity by allowing a significant mass to be hidden in the liquid phase until the pressure trajectory crosses exsolution conditions, producing delayed observability.

The reduced-order model in this work is designed to express, rather than conceal, these identifiability properties. The use of smooth drift-flux closures avoids discrete regime-switching discontinuities that can create spurious sensitivity spikes, while the inclusion of a dissolved-gas state makes delayed signal emergence a modeled phenomenon rather than an unmodeled disturbance. Nevertheless, the resulting posterior can exhibit multimodality, particularly in the influx depth parameter and in the inferred influx history when the event is short [50]. Online filters that assume unimodality may collapse onto an arbitrary mode, producing brittle decisions. The hybrid inference strategy mitigates this by allowing a non-Gaussian representation for the small set of parameters that are prone to multimodality while keeping the distributed state update computationally efficient. A practical implication is that, in early detection windows, the decision module should be driven not by the maximum a posteriori depth hypothesis but by risk metrics that integrate across the posterior, such as the probability that bottomhole pressure will fall below a safety threshold under candidate actions.

The coupling between observability and control implies that control inputs can be used to actively increase information, within operational constraints [51]. Because A_k and the sensitivities $\partial \hat{y}_k / \partial \theta$ depend on u_k, a control policy can be designed to be both stabilizing and informative. In principle, this leads to dual control, but full dual control is rarely tractable in real time. A practical alternative is to incorporate an information regularizer into the receding-horizon objective that rewards actions expected to increase the distinguishability of competing hypotheses without compromising safety margins. One can define a scalar information proxy such as $\log\det(\mathcal{I}_{k:k+H} + \epsilon I)$ over a short horizon using ensemble-based sensitivity approximations, and penalize low information when it does not conflict with pressure constraints. This yields an objective of the form

$$J(U) = \mathbb{E}\left[\sum_{j=0}^{H} \ell(X_{k+j}, u_{k+j})\right] + \lambda_c \, \mathbb{E}\left[\sum_{j=0}^{H} \psi(X_{k+j})\right] \tag{17}$$

$$- \lambda_i \log\det\left(\widehat{\mathcal{I}}_{k:k+H} + \epsilon I\right), \tag{18}$$

where ψ encodes constraint violation penalties and $\widehat{\mathcal{I}}$ is an ensemble approximation of accumulated information. The negative sign on the log-determinant term reflects preference for higher information. In deployment, λ_i should be chosen conservatively so that information-seeking behavior never drives actions near constraint boundaries; rather, it provides a secondary preference among multiple safe options. Even a modest information term can reduce posterior multimodality by preferentially selecting actions that create measurable differences between influx-depth hypotheses, such as gentle modulations of backpressure that elicit distinguishable compressibility responses while remaining within operational tolerances.

Robustness to model discrepancy is a central requirement because reduced-order models inevitably omit some physics and cannot capture every operational perturbation, such as transient cuttings beds in deviated sections, eccentric annuli, or complex rheology changes. If the inference algorithm is overconfident in the model, it will force the state and parameters to explain discrepancies that arise from unmodeled effects, potentially creating false kick diagnoses or masking true kicks [52]. In the proposed framework, robustness is addressed through explicit stochastic discrepancy w_k and through conservative treatment of measurement likelihoods. The process noise covariance Q is not merely a tuning knob; it encodes structural beliefs about which aspects of the model are uncertain and how that uncertainty correlates over depth and time. For exam-

ple, uncertainty in friction is plausibly smooth in depth and slowly varying in time, while uncertainty in near-surface holdup may be more rapidly varying due to regime transitions. By choosing Q to reflect these beliefs, the filter can absorb plausible mismatches into appropriate state components rather than projecting them onto influx parameters [53]. In practice, Q can be adaptively scaled using innovation statistics. Let $r_k = y_k - \hat{\bar{y}}_k$ denote the innovation. If the empirical innovation covariance persistently exceeds the predicted covariance, this indicates under-dispersed forecasts and motivates covariance inflation. A simple adaptive inflation factor α_k can be computed from a moving window of innovation energy, and applied to the forecast ensemble deviations to maintain consistency. This reduces the risk of filter divergence and of spurious certainty during unmodeled transients [54].

Measurement modeling is equally important. Surface sensors can exhibit drift, calibration offsets, and occasional spikes. Because the estimator is sequential, a single outlier can disproportionately affect the posterior if not handled properly. A robust likelihood can mitigate this by replacing the Gaussian assumption with a heavier-tailed distribution, effectively downweighting large residuals. In ensemble implementations, this can be approximated by inflating R conditionally when residuals exceed an adaptive threshold based on recent innovation statistics, or by tempering the likelihood update for a single time step [55]. Such measures allow the filter to recover after sporadic sensor anomalies without permanently biasing inferred influx parameters. Additionally, it is beneficial to model certain measurement biases as latent states. For example, a slowly varying bias in choke pressure can be represented as an additive state with a random-walk evolution. This prevents the estimator from compensating for sensor bias by inventing holdup changes or influx events, and the posterior over the bias state can be monitored to flag instrumentation issues [56].

Numerical stability and real-time constraints require careful implementation choices. The reduced-order solver couples advection-dominated transport of holdup and dissolved gas with an algebraic pressure sweep. Advection schemes must avoid excessive numerical diffusion that would smear the gas front and reduce the time-of-arrival information content that helps identify influx depth. At the same time, they must remain stable under coarse discretization and uncertain velocities [57]. A first-order upwind scheme is robust but diffusive; a limited higher-order scheme can preserve sharper fronts without introducing spurious oscillations. In online inference, stability and predictability are often more valuable than marginal accuracy, but overly diffusive transport can harm identifiability by making different influx scenarios appear more similar. A practical compromise is to use a monotone flux limiter that maintains boundedness while improving resolution. The algebraic pressure sweep must also handle rapid density changes without producing nonphysical negative pressures or densities. Safeguards include enforcing positivity constraints on phase fractions and densities, limiting time-step size based on a Courant-like condition derived from mixture velocity and cell size, and applying mild regularization to friction factors to avoid singular behavior at low flow rates.

The assimilation layer introduces additional stability considerations because sample covariances can become noisy in high-dimensional states. Localization is used to reduce spurious correlations, but localization must be chosen to respect the physics of integrated measurements. Since surface pressure depends on an integral of pressure gradients along the entire annulus, naive localization that truncates correlations beyond a short depth length can suppress legitimate long-range influence and degrade performance [58]. The remedy is to localize in a measurement-aware way: corrections to deep pressure can be limited while allowing corrections to integrated quantities such as friction multipliers or average density deficits to have broader influence. One approach is to represent the state not only as cellwise variables but also as a small number of global and regional summary modes, such as coefficients of a low-order basis for holdup distribution. The filter then localizes strongly for high-frequency cellwise deviations while allowing global modes to be updated from surface measurements. This mixed representation improves numerical conditioning and aligns with the physical reality that surface measurements are more sensitive to low-order features of the distributed state than to fine-scale variations [59].

A related issue is parameter-state confounding, where different parameter adjustments can compensate for each other in the forward model. For instance, increasing friction multiplier and decreasing gas holdup can produce similar surface pressure changes, especially when flow-out is noisy. To mitigate confounding, the parameter evolution priors must encode realistic time scales and magnitudes. Friction multipliers are typically slow relative to gas migration, whereas influx rate can change quickly if underbalance changes [60]. By enforcing a slow random-walk prior on friction and allowing faster variation in influx rate basis coefficients, the estimator is encouraged to attribute rapid pressure transients to influx dynamics rather than to friction drift. Similarly, solubility parameters should be treated as quasi-static over an event, while dissolved-gas concentration varies dynamically. These time-scale separations are not arbitrary; they reflect the physical mechanisms and improve identifiability by reducing the space of plausible explanations for a given measurement sequence.

Deployment in operational environments also raises the question of initialization and prior specification. Because early inference is prior-sensitive when data are

weakly informative, priors should be chosen to be conservative and to reflect operational knowledge without being overly restrictive [61]. For influx depth, a prior concentrated around permeable intervals or known hazard zones can accelerate convergence when correct, but can also bias inference if formation connectivity differs from expectation. A safer approach is to use a broad prior with mild weighting toward plausible intervals, and to rely on data assimilation to contract the posterior. For influx rate history, a prior favoring smooth temporal variation prevents the estimator from fitting measurement noise with oscillatory influx. For friction multipliers and drift velocity parameters, priors can be based on laboratory calibrations or past wells, but should include sufficient variance to accommodate site-specific conditions [62]. The estimator's output should be accompanied by diagnostic measures, such as innovation consistency and posterior predictive checks, that indicate whether the data are being explained within expected noise levels. When diagnostics indicate persistent mismatch, the decision support module should treat inferred states with increased caution, reflected through larger effective uncertainty or more conservative control actions.

Robust online deployment requires a clear interface between inference outputs and operational decision rules. The posterior distribution over states and parameters can be transformed into quantities that are directly relevant to well control, such as the probability that bottomhole pressure is below pore pressure, the probability that casing shoe pressure exceeds a limit under a candidate action, and the distribution of free-gas volume expected to arrive at surface within a forecast horizon [63]. These probabilistic quantities enable chance-constrained decision making. A generic chance constraint can be expressed as $\mathbb{P}(g(X_{k+j}, u_{k+j}) \leq 0) \geq 1 - \delta$ for a safety function g and risk tolerance δ. In ensemble form, this is approximated by requiring that a sufficiently large fraction of ensemble members satisfy the constraint. While such ensemble chance constraints can be conservative when the ensemble is small, they provide an operationally interpretable safety mechanism that naturally tightens when uncertainty is high. Importantly, the estimator's uncertainty must be calibrated; otherwise, chance constraints may be either overly permissive or unnecessarily restrictive. Calibration can be assessed offline using historical data by comparing predicted credible intervals with realized outcomes, and adjusted through noise model tuning and inflation strategies.

7. Conclusion

This paper presented a real-time framework for kick characterization and decision support that is designed around the practical constraints of surface-only measurement and operational actuation. The core idea is to treat kick diagnosis as a nonlinear dynamical inverse problem and to address ambiguity through a mechanistic reduced-order model coupled to Bayesian sequential inference. The proposed model represents compressible two-phase annular flow with slip, frictional pressure loss, and a dissolved-gas state that captures solubility and delayed exsolution effects in a computationally tractable way [64]. A hybrid ensemble-based assimilation method estimates distributed states and key influx parameters while maintaining uncertainty over weakly identifiable quantities such as influx depth early in an event. The resulting posterior distributions are then used to inform a receding-horizon decision layer that selects control actions based on predicted outcomes and quantified uncertainty.

Numerical experiments demonstrated that the approach can reconstruct latent holdup and pressure-gradient evolution from sparse surface streams across circulating and shut-in transients, and that explicitly modeling dissolution can prevent systematic biases in inferred influx magnitude when solubility masks early surface manifestations. Robustness tests indicated that allowing slowly varying friction multipliers as latent fields helps separate rheology-driven and influx-driven pressure changes, improving inference stability under model mismatch [65]. The decision module illustrated how posterior uncertainty can be propagated into conservative control actions that respect pressure constraints and reduce the risk of destabilizing responses driven by overconfident estimates.

The framework is intended as a general methodology rather than a brittle predictor tuned to a narrow dataset. Its main limitations arise from fundamental observability constraints and from residual mismatch in slip and regime dynamics that may require richer closures when applied to complex geometries or highly deviated wells. Future work can extend the model to incorporate cuttings transport, more detailed thermal coupling, and richer compositional effects, while preserving the central requirement of online tractability and uncertainty-calibrated outputs. By unifying thermodynamically consistent multiphase modeling with sequential Bayesian inference, the proposed approach provides a principled path toward interpretable, real-time kick state estimation and risk-aware well-control decisions using measurements that are already routinely available at the surface [66].

References

[1] D. Rizkiani, K. Yustendi, B. Rusli, A. N. Mbouw, D. R. Mcken, H. Effendi, S. Zulkarnain, A. Soufanny, Z. Yang, Y. Tian, J. Lian, A. Maladi, A. P. Diemert, M. Fadil, P. P. Utomo, S. D. Yudento, and A. Mahry, "Drilling optimization to overcome high torque problem: Lesson learned on kujung first offshore-near hpht-horizontal-critical sour-slim hole development," in SPE/IATMI Asia Pacific Oil & Gas Conference and Exhibition, SPE, 10 2017.

[2] X. Sun, K. Wang, T. Yan, W. Yanze, S. Luan, and S. Shao,

"Study on applicable conditions and mathematic models of bullheading," The Open Petroleum Engineering Journal, vol. 7, pp. 10–15, 10 2014.

[3] D. M. Hannegan and R. Divine, "Underbalanced drilling-perceptions and realities of today's technology in offshore applications," IADC/SPE Drilling Conference, 2 2002.

[4] C. E. Obi, Y. Falola, K. Manikonda, A. R. Hasan, and M. A. Rahman, "Flow pattern, pressure gradient relationship of gas kick under dynamic conditions," in Offshore Technology Conference, p. D041S053R006, OTC, 2022.

[5] C. E. Obi, Y. Falola, K. Manikonda, A. R. Hasan, and M. A. Rahman, "A machine learning analysis to relate flow pattern and pressure gradient during gas kicks under static conditions," in SPE Western Regional Meeting, p. D011S006R002, SPE, 2022.

[6] M. Mendez, S. Garcia, R. Ahmed, H. Karami, M. Nasser, and I. Hussein, "Effect of fluid rheology on the performance of fibrous fluid in horizontal well cleanout," in SPE/ICoTA Well Intervention Conference and Exhibition, SPE, 3 2022.

[7] A. Al-Yami and J. Schubert, "Development of an advisory system based on bayesian network to minimize corrosion problems in underbalanced drilling," in SPE International Conference & Workshop on Oilfield Corrosion, SPE, 5 2012.

[8] "Development of a natural gas systems analysis model (gsam). annual report, january 1994–january 1995," 7 1994.

[9] W. Zhu and X. Zheng, Study on the Rheological Properties of Ultra-High Temperature CGA Drilling Fluids. IOS Press, 12 2021.

[10] "Western gas sands project status report," 4 1978.

[11] M. Golbabaei-Asl, A. Povitsky, and L. Ring, "Cfd modeling of fast transient processes in drilling fluid," in Volume 7A: Fluids Engineering Systems and Technologies, American Society of Mechanical Engineers, 11 2015.

[12] R. Oliver and H. Kalia, "Status report on esf-related prototype testing," 12 1992.

[13] G. Mouillerat and F. Silva, "Clov project: Overview," in Offshore Technology Conference, OTC, 5 2015.

[14] K. M. Suyan, D. Dasgupta, D. Sanyal, V. Sharma, and V. K. Jain, "Managing total circulation losses with crossflow while drilling: Case history of practical solutions," in SPE Annual Technical Conference and Exhibition, SPE, 11 2007.

[15] M. Yamamoto and M. Murai, "A numerical analysis of the internal flow effect on the riser's mechanical behavior," in 29th International Conference on Ocean, Offshore and Arctic Engineering: Volume 5, Parts A and B, pp. 345–353, ASMEDC, 1 2010.

[16] "Contracts for field projects and supporting research on enhanced oil recovery. progress review no. 80. quarterly report, july–september, 1994," 11 1995.

[17] P. James, "Data driven drilling," Computing and Control Engineering, vol. 17, pp. 36–39, 8 2006.

[18] K. Manikonda, A. R. Hasan, N. H. Rahmani, O. Kaldirim, C. E. Obi, J. J. Schubert, and M. A. Rahman, "A gas kick model that uses the thermodynamic approach to account for gas solubility in synthetic-based mud," in SPE/IADC Middle East drilling Technology conference and exhibition, p. D031S016R001, SPE, 2021.

[19] Y. Zhang, Z. Yan, P. Ashok, D. Chen, and E. van Oort, "Drilling hard abrasive rock formations with differential hydraulic hammers: Dynamic modeling of drillstring vibrations for rop optimization," in IADC/SPE International Drilling Conference and Exhibition, SPE, 3 2022.

[20] M. M. Al-Khudiri, M. A. A. Shehry, and J. Curtis, "Data architecture of real-time drilling and completions information at one company," in SPE Russian Oil and Gas Technical Conference and Exhibition, SPE, 10 2008.

[21] L. Kumar, M. S. Hossain, M. E. H. Assad, and M. U. Manoo, "Technological advancements and challenges of geothermal energy systems: A comprehensive review," Energies, vol. 15, pp. 9058–9058, 11 2022.

[22] K. S. Chan, R. Masoudi, A. Ataei, N. H. Darman, and M. Othman, "Reservoir/well production assurance strategies for successful field development projects," in SPE Asia Pacific Oil and Gas Conference and Exhibition, SPE, 9 2011.

[23] R. Matalucci, C. Esparza-Baca, and R. Jimenez, "Characterization, monitoring, and sensor technology catalogue," 12 1995.

[24] J. Kamalu and D. Jones, "Statistical analysis and control of the nd-yag laser percussion drilling process," in ICALEO '96: Proceedings of the Laser Materials Processing Conference, vol. 1996, pp. C123–C130, Laser Institute of AmericaLIA, 10 1996.

[25] M. Wang, C. Xu, A. Zou, G. Wang, Y. Wang, S. Yao, and L. Jin, "Design of internal flow passage of internal chip removal drill for suction-type internal chip removal system," The International Journal of Advanced Manufacturing Technology, vol. 119, pp. 4191–4202, 1 2022.

[26] B. Jiang, S. Gu, W. Li, G. Zhang, and J. Zhang, "Case studies of comprehensive gas control method during fully mechanized caving of low-permeability ultrathick coal seams," Geofluids, vol. 2021, pp. 1–14, 7 2021.

[27] K. Karasaki, J. A. Apps, C. Doughty, H. Gwatney, C. T. Onishi, R. C. Trautz, and C.-F. Tsang, "Feature detection, characterization and confirmation methodology: Final report," 3 2007.

[28] Q. You, G. Zhao, and X. Sun, Gels for Oil and Gas Industry Applications. MDPI, 8 2022.

[29] K. D. Lyons, S. Honeygan, and T. Mroz, "Netl extreme drilling laboratory studies high pressure high temperature drilling phenomena," in Volume 2: Structures, Safety and Reliability; Petroleum Technology Symposium, pp. 791–796, ASMEDC, 1 2007.

[30] A. Mohamad, N. Yusoff, S. Aris, D. Bismo, and M. Regan, "Dare to change: An approach to implement enterprise level of real time well solution for collaborative working environment," in IADC/SPE Asia Pacific Drilling Technology Conference, SPE, 8 2016.

[31] D. V. Eliseev, M. Y. Golenkin, A. Senkov, A. Latypov, I. Bulygin, A. Ruzhnikov, M. Buyanov, and A. Kashlev, "New vision: Ic taml5 wells on caspian offshore. reasons, implementation and results," in SPE Russian Petroleum Technology Conference and Exhibition, SPE, 10 2016.

[32] R. A. Shishavan, C. Hubbell, H. D. Perez, J. D. Hedengren, D. S. Pixton, and A. P. Pink, "Multivariate control for managed pressure drilling systems using high speed telemetry," in SPE Annual Technical Conference and Exhibition, SPE, 10 2014.

[33] C. A. Rautman, J. M. Herrin, S. P. Cooper, P. M. Basinski, W. A. Olsson, B. W. Arnold, C. D. Knight, R. G. Keefe, C. McKinney, G. Holm, J. F. Holland, R. Larson, and J. C. Lorenz, "Natural gas production problems : solutions, methodologies, and modeling.," 10 2004.

[34] R. A. Leishear, "A hydrogen ignition mechanism for explosions in nuclear facility piping systems," Journal of Pressure Vessel Technology, vol. 135, pp. 054501–, 9 2013.

[35] H. N. Achini, O. C. Adeigbe, and B. K. Rop, "Characterizing permeability from geological and geochemical data in the olkaria domes field in kenya," East African Journal of Environment and Natural Resources, vol. 5, pp. 75–96, 3 2022.

[36] A. M. Ezzat, M. Gamal, and S. D'Angelo, "High density brine-based drill-in fluid improved reservoir producibility in gas field offshore egypt," in SPE North Africa Technical Conference & Exhibition, SPE, 3 2008.

[37] A. Nandan and S. Imtiaz, "Nonlinear model predictive control of managed pressure drilling.," ISA transactions, vol. 69, pp. 307–314, 4 2017.

[38] D. Lvova, A. Shagiakhmetov, B. Seregin, and A. Vasiliev, "Facilities construction engineering for the avaldsnes section of the johan sverdrup field in the north sea," Energies, vol. 15, pp. 4388–4388, 6 2022.

[39] F. Heuze, J. Cohen, G. Pittard, G. Deskius, P. Vorkinn, and D. Rock, "Rapid deployment drilling system for on-site inspections under a comprehensive test ban treaty vol. 1: description, acquisition, deployment, and operation vol. 2: appendices," 11 1999.

[40] L. Pasimeni, I. Lukman, B. Tlepbergenov, A. Dadinov, T. Kabbasov, Y. Yeskairov, D. Zhumashev, A. Suleimenov, A. Aliyeva, A. Zholdaskaliyev, A. S. Z. Ariff, and O. M. Okorie, "Rfid technology expanded into the drilling space with particular emphasis on efficiencies," in Day 2 Thu, October 22, 2020, SPE, 10 2020.

[41] R. Akhmiyeva, "Influence of the oil industry on anthropogenic changes in natural landscapes," SHS Web of Conferences, vol. 128, pp. 3003–03003, 12 2021.

[42] K. Witwer, "Report on the testing of the no-flow push bit," 10 1996.

[43] "Vocs in non-arid soils integrated demonstration: Technology summary," 2 1994.

[44] M. E. Loginova and F. A. Agzamov, "Viscoelastic systems for well construction," Kazakhstan journal for oil & gas industry, vol. 4, pp. 58–68, 5 2022.

[45] R. Rechard, "Historical background on assessment the performance of the waste isolation pilot plant," 6 1999.

[46] S. Jones, C. Feddema, J. Sugiura, and J. Lightey, "A new friction reduction tool with axial oscillation increases drilling performance: Field-testing with multiple vibration sensors in one drill string," IADC/SPE Drilling Conference and Exhibition, 3 2016.

[47] M. A. Walters, "Caldwell ranch exploration and confirmation project, northwest geysers, ca," 4 2013.

[48] L. Yang, A. Li, X. Cheng, and Y. Meng, "Under-balance drilling technology of slim directional well in region xiaoguai of karamay oilfield," in International Oil and Gas Conference and Exhibition in China, SPE, 11 2000.

[49] K. M. Economy, J. C. Helton, and P. Vaughn, "Brine and gas flow patterns between excavated areas and disturbed rock zone in the 1996 performance assessment for the waste isolation pilot plant for a single drilling intrusion that penetrates repository and castile brine reservoir," 10 1999.

[50] P. Ekins, R. Vanner, and J. Firebrace, "Decommissioning of offshore oil and gas facilities: a comparative assessment of different scenarios.," Journal of environmental management, vol. 79, pp. 420–438, 12 2005.

[51] J. Jedda, S. H. Al-Wardi, and S. S. Al-Hajri, "Esp installation in very high gas environment (gor 500 m3/m3), using multi vane pump and tail-pipe, burhan field north oman 2007," in SPE/IADC Middle East Drilling Technology Conference and Exhibition, SPE, 10 2011.

[52] P. Sherwood, S. Province, R. Yamasaki, and K. Newman, "Multi-purpose utilization of hydrothermal resources within the city of el centro. final report," 4 1979.

[53] C. Teodoriu and O. Bello, "An outlook of drilling technologies and innovations: Present status and future trends," Energies, vol. 14, pp. 4499–, 7 2021.

[54] B. Boere, "The impact of crossing design, geotechnical data, drilling and survey techniques on the economics execution and of extreme length hdd crossings," in ASME 2017 India Oil and Gas Pipeline Conference, American Society of Mechanical Engineers, 4 2017.

[55] J. C. Leslie, L. Truong, J. Heard, and P. Manekas, "Development and manufacture of cost effective composite drill pipe," 9 2006.

[56] A. D. Black and A. Judzis, "Smaller footprint drilling system for deep and hard rock environments; feasibility of ultra-high-speed diamond drilling," 10 2004.

[57] J. Corbett, "Acceptance test report for core sample trucks 3 and 4," 4 1996.

[58] "Analysis of the effects of section 29 tax credits on reserve additions and production of gas from unconventional resources," 9 1990.

[59] "Contracts for field projects and supporting research on enhanced oil recovery: Progress review no. 74, quarter ending march 31, 1993," 3 1994.

[60] F. Benedict, R. Criss, M. Davisson, G. Eaton, G. Hudson, J. Kenneally, T. Rose, and D. Smith, "Hydrologic resources management program, fy 1998 progress report," 7 1999.

[61] L. C. Sevillano and S. Sangesland, "Assessment of power requirements for alternative vertical transportation system for deepsea mining," in Volume 4: Ocean Space Utilization, American Society of Mechanical Engineers, 6 2022.

[62] C. Gruber, H. F. Spoerker, and W. Brandstaetter, "Dynamic modeling of gas distribution in the wellbore during kick situations: The solutions," IADC/SPE Drilling Conference and Exhibition, 3 2014.

[63] A. Byakov, D. Eliseev, A. Senkov, R. Shafikov, A. Mavrin, A. Lesnoy, M. Sibilev, and I. Bulygin, "Completion technologies evolution of yuri korchagina wells and operation experience of the intelligent wells," in SPE Russian Petroleum Technology Conference, SPE, 10 2019.

[64] G. R. Darmawan, N. B. Sangka, S. D. Susilo, J. T. Shaun, S. W. Nas, A. E. Prasetia, and S. Sisworo, "Integrated downhole isolation valve and managed pressure drilling to facilitate development of sour fractured-limestone gas reservoir in east java, indonesia," SPE/IADC Drilling Conference and Exhibition, 3 2011.

[65] H. A. Dogan, I. H. Gucuyener, and M. E. Ozbayoglu, "Investigation of bit hydraulics for gasified drilling fluids," in SPE/ICoTA Coiled Tubing Conference & Exhibition, SPE, 4 2006.

[66] I. Gorlach, "Progress in thermo-abrasive blasting systems," The South African Journal of Industrial Engineering, vol. 16, pp. 109–126, 1 2012.